

PAPER

Effect of B-site cation ordering on high temperature thermoelectric behavior of $\text{Ba}_x\text{Sr}_{2-x}\text{TiFeO}_6$ double perovskites

To cite this article: Deepankar Sri Gyan *et al* 2020 *J. Phys.: Condens. Matter* **32** 235401

View the [article online](#) for updates and enhancements.



IOP | ebooks™

Bringing together innovative digital publishing with leading authors from the global scientific community.

Start exploring the collection—download the first chapter of every title for free.

Effect of B-site cation ordering on high temperature thermoelectric behavior of $\text{Ba}_x\text{Sr}_{2-x}\text{TiFeO}_6$ double perovskites

Deepankar Sri Gyan^{1,5}, Vivek Sundram^{2,3,5}, Akansha Dwivedi¹ ,
Somnath Bhowmick³ and Tanmoy Maiti^{2,3,4} 

¹ Department of Ceramic Engineering, Indian Institute of Technology (BHU), Varanasi, UP, 221005, India

² Plasmonics and Perovskites Laboratory, Indian Institute of Technology, Kanpur, UP, 208016, India

³ Department of Materials Science and Engineering, Indian Institute of Technology, Kanpur, UP, 208016, India

E-mail: tmaiti@iitk.ac.in (Tanmoy Maiti), bsomnath@iitk.ac.in (Somnath Bhowmick)
and akanshadwivedi.cer@itbhu.ac.in (Akansha Dwivedi)

Received 28 September 2019, revised 27 January 2020

Accepted for publication 12 February 2020


Published 10 March 2020



Abstract

Here, we have reported the detailed structural analysis in correlation with thermoelectric properties of Ba doped $\text{Sr}_2\text{TiFeO}_6$ (BSTF) double perovskites in the temperature range from 300 K to 1100 K. BSTF compositions exhibit single phase cubic structure with $Pm\bar{3}m$ crystal symmetry from room temperature to 523 K and also at temperature beyond 923 K. Rietveld refinement of high temperature XRD data suggests the coexistence of two cubic phases with $Pm\bar{3}m$ space group having same composition in the intermediate temperature region. Correlation of the phase-fraction with electrical conductivity data posits the possibility of high temperature cubic phase being conductive compared to the insulator-like cubic phase observed at room temperature. The experimental analysis alone seems insufficient to explain the conductivity behavior demonstrating semiconductor ($d\sigma/dT > 0$) to metal like ($d\sigma/dT < 0$) transition. Hence DFT framework has been adopted for computational analysis coupled with the Boltzmann transport equations to understand their thermoelectric properties based on the electronic restructuring occurred due to octahedral arrangements in these double perovskites. It has been shown that clustering of FeO_6 octahedra may lead to the formation of a conduction path in the cubic phase of BSTF, which induces metallic behavior in these double perovskites.

Keywords: thermoelectric, octahedral arrangement, Rietveld refinement, density functional theory, BoltzTrap

 Supplementary material for this article is available [online](#)

(Some figures may appear in colour only in the online journal)

1. Introduction

Over the last few decades, $\text{A}_2\text{B}'\text{B}''\text{O}_6$ double perovskites demonstrated exotic properties due to their wide range of crystal symmetry as well as electronic structures ranging from insulating to metal like and even sometimes half metallic with

spin-polarized electrical conductivity [1–3]. Further, cation doping in double perovskite offers more flexibility to tailor the electrical properties of these complex oxides. Such vividness in properties is largely controlled by structural ordering, valance state and spin states of B' and B'' cations [4]. In the recent past, double perovskite oxides showed promises for high temperature thermoelectric applications [5–10]. The working principle of thermoelectric power generator relies on the Seebeck effect to convert thermal energy into electricity

⁴ Author to whom any correspondence should be addressed.

⁵ Equal contribution.

and the energy conversion efficiency is determined by a dimensionless figure of merit, defined as; $ZT = \frac{S^2\sigma}{\kappa}$, where, σ , S and κ are electrical conductivity, Seebeck coefficient and thermal conductivity, respectively [11]. Double perovskites-based oxide thermoelectrics have the advantage of low processing cost, better stability at high temperature compared to state-of-the-art materials like chalcogenides and intermetallics although their ZT values need to be improved. Recently, environmentally friendly, rare-earth free $Ba_xSr_{2-x}TiB'O_6$ ($B' = Fe, Co, Mo$) based double perovskites [6–9] showed great potentials for thermoelectric applications. Earlier, authors reported that large thermopower ($\sim 800 \mu V K^{-1}$) can be obtained in $Ba_xSr_{2-x}TiB'O_6$ based double perovskites when B' site is occupied by ferromagnetic iron [6]. Moreover, an interesting phenomenon was observed in the temperature dependent electrical conductivity of $Ba_xSr_{2-x}TiFeO_6$ (BSTF) double perovskites indicating a semiconductor ($d\sigma/dT > 0$) to metal like ($d\sigma/dT < 0$) transition [6, 7]. A similar kind of semiconductor to metal transition was observed in some charge-ordered perovskite and double perovskite halides, such as $Cs_2Au_2X_6$, $Cs_2In(I)In(III)Cl_6$, $AlInX_3$, etc, but those are pressure driven instead of temperature [12–14]. However, in case of BSTF system, it could not be termed as metallic, because the conductivity obtained was on the order of $100 S m^{-1}$, which is too low to predict any metallic behavior. Although the charge transport mechanism was explained using the small polaron hopping conduction model, no conclusion was drawn explaining the electrical conductivity behavior of these BSTF compounds, which showed insulating, semiconductor and metal-like behaviors in various temperature ranges. In order to get a clear insight into such semiconductor to metal-like transition, in the present work we carried out detailed structural investigations by high temperature x-ray diffraction analysis on $Ba_xSr_{2-x}TiFeO_6$ ($x = 0.0, 0.1$) compounds in order to access its structural changes with temperature in correlation with the change in thermoelectric parameters. Also, detailed computational analysis using DFT and BoltzTraP was performed to study the effects of B-cation ordering on the thermoelectric properties of these double perovskites. With the double perovskites showing cubic structure with $Pm\bar{3}m$ space group, all possible octahedral configurations were considered in a finite periodic box and each phase showing variable properties was accounted for. Local clustering of octahedral arrangements in these double perovskites was found to be responsible for inducing a new cubic phase with $Pm\bar{3}m$ space group which is metallic in nature, resulting the semiconductor to metal transition observed in temperature dependent conductivity behavior.

2. Experimental

2.1. Theoretical simulation

Structural optimizations and electronic band structure calculations were performed using the density functional theory (DFT), as implemented in the quantum espresso package [15], using ultra soft pseudopotentials and GGA-PBE

exchange correlation function [16]. A $(2 \times 2 \times 2)$ unit cell (consisting of 40 atoms) of perovskite $SrTiO_3$ was chosen, with 50% of the Ti replaced by Fe (STF). This was done to preserve the cubic symmetry of the material. Furthermore, Ba doping was introduced in place of Sr with the chemical formula $Ba_{0.25}Sr_{1.75}TiFeO_6$ (BSTF). A variable cell relaxation was carried out on both STF and BSTF, using a $10 \times 10 \times 10$ k-mesh Monkhorst pack grid. The lattice parameters were taken from the XRD data obtained from the experiments. The kinetic energy cut-off and charge density cut-off were set to 40 Ry and 400 Ry respectively. The convergence criteria were set to be 10^{-6} Ry energy difference between successive steps and 10^{-3} Ry/Bohr force on each atom. The electronic band structures were plotted along $\Gamma-X-M-\Gamma-R-X$ points [17]. The semi-classical Boltzmann theory, as implemented in the BoltzTraP [18] package, was used to predict the transport properties of STF and BSTF in the temperature range from 300 K to 1100 K. It is to be noted that the BoltzTraP code uses a constant relaxation time approach and we have used τ as a parameter. The temperature dependence of the transport properties was modelled using the Fermi-Dirac distribution. The input for the BoltzTraP was provided from DFT, using the non-self-consistent calculations, using a set of 8000 k -points to sample the IBZ.

2.1.1. Sample preparation and characterizations. $Ba_xSr_{2-x}TiFeO_6$ ($0 \leq x \leq 0.25$) compositions were synthesized using conventional solid-state synthesis route. Stoichiometric amount of $BaCO_3$ (Sigma Aldrich $\geq 99\%$), $SrCO_3$ (Sigma Aldrich $\geq 99.9\%$), TiO_2 (Sigma Aldrich $\geq 99.5\%$) and Fe_2O_3 (Sigma Aldrich $\geq 99.995\%$) were mixed and milled in a roller pot mill for 24 h using zirconia balls and acetone as mixing medium. After that the slurry was dried and obtained powder was calcined at 1473 °C for 10 h in order to achieve single phase double perovskite. Now the calcined powders were again milled in Fritsch®, PULVERISSETTE 7 premium Line planetary mill at 600 RPM for 8 h using zirconia balls and ethanol as a medium in order to obtain nanopowders. The obtained nanopowders were mixed with 2% PVA solution and pressed in the form of cylindrical pellets. These pellets were sintered at 1623 K for 10 h in order to get dense ceramic samples.

Sintered pellets were crushed in the form of powder to perform powder diffraction analysis at room temperature as well as higher temperature in order to examine structural behavior of the double perovskites. XRD data was collected using Rigaku high resolution x-ray diffractometer and the patterns were recorded in 2θ range of $10-100^\circ$ in temperature range 300–1173 K. Rietveld refinement was carried out on all the diffraction patterns, using Full prof suit, in order to examine change in structural behavior with temperature. Microstructural investigations were carried out on a polished sintered pellet using Scanning Electron microscope (Carl Zeiss NTS GmbH, EV050, Germany). The sintered pellets were polished and subjected to ZEM-3M10 apparatus (ULVAC-RIKO Inc.) to measure their electrical conductivity and Seebeck coefficient in temperature range 300–1173 K.

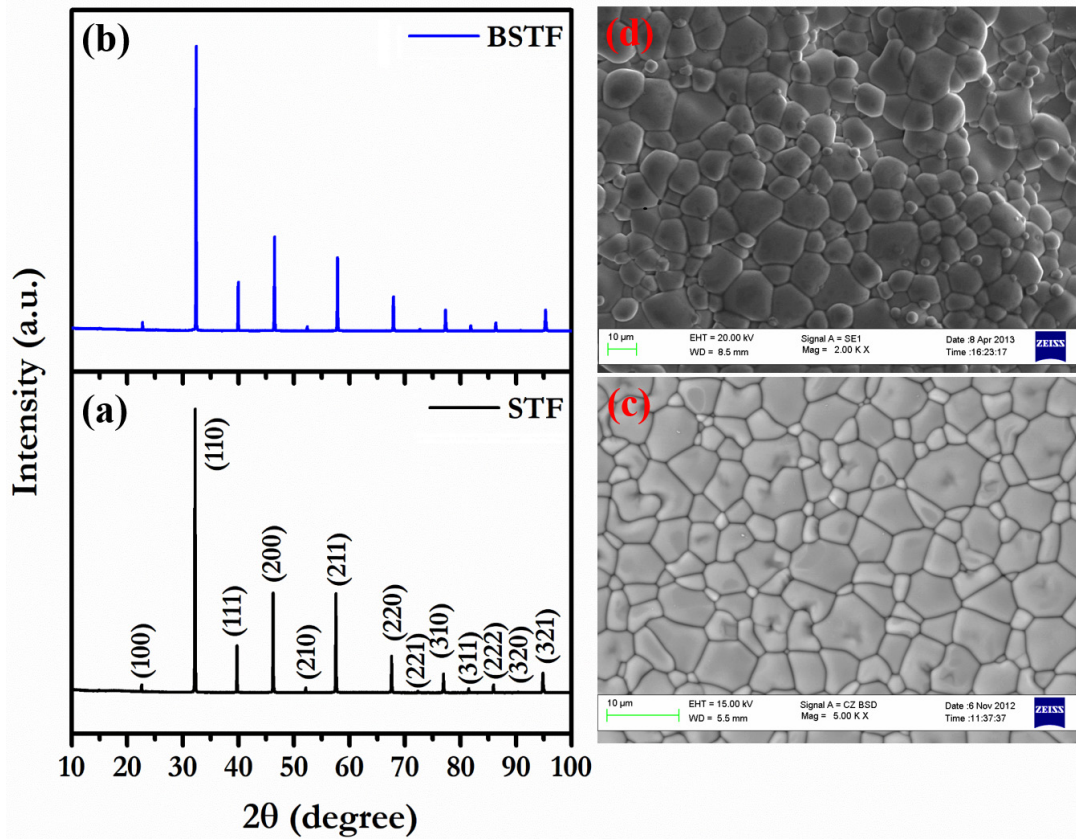


Figure 1. Room temperature x-ray diffraction patterns of (a) STF and (b) BSTF; SEM image of polished surface of (c) STF and (d) BSTF ceramics.

3. Results and discussion

3.1. Structural and microstructural analysis

Figures 1(a) and (b) depict the room temperature XRD patterns of $\text{Sr}_2\text{TiFeO}_6$ (STF) and $\text{Ba}_{0.1}\text{Sr}_{1.9}\text{TiFeO}_6$ (BSTF), respectively. All the peaks in diffraction patterns were indexed as per cubic perovskite structure with $Pm\bar{3}m$ space group. Presence of no extra peaks suggests the phase purity of all the compositions. Microstructural analysis was carried out using scanning electron microscope in order to check the density and grain growth of the sintered samples. The SEM micrographs of STF and BSTF are displayed in figures 1(c) and (d), respectively. Dense microstructure with no such porosity with uniform grain growth was observed for all the compositions. Grain size was estimated by using ImageJ software. The average grain size was increased from $4.82 \mu\text{m}$ for STF to $7.42 \mu\text{m}$ for BSTF, suggesting that the inclusion of Ba^{2+} ion in the unit cell of STF enhanced the grain growth.

3.2. Variation in structure at elevated temperature range

In order to examine the signature of any high temperature phase transition of BSTF compositions, high temperature x-ray diffraction analysis was performed in temperature range 300–1173 K. STF showed cubic double perovskite structure with cubic $Pm\bar{3}m$ configuration at room temperature. As temperature was raised, the diffraction pattern continued to be

cubic phase with same $Pm\bar{3}m$ configuration with slight shift in the peak positions which might be the results of lattice elongation due to thermal expansion. Such behavior was observed in the temperature range from 300 K to 573 K. Similar type of single-phase cubic behavior having $Pm\bar{3}m$ configuration, with increasing lattice parameter, was observed beyond 923 K as well. But in intermediate range of temperature, i.e. from 573 K to 923 K, diffraction peaks correspond to each plane started showing splitting suggesting some sort of structural transition in this temperature range. Similar behavior was observed for the BSTF composition with the peak splitting behavior in temperature range of 673 K–973 K. On the basis of these observations, the study of STF and BSTF compositions was divided in three zones with different temperature range namely Zone 1, Zone 2 and Zone 3. Rietveld refinement was carried out on the diffraction patterns observed in zone 1 and zone 3 temperature range for both STF and BSTF with respect to $Pm\bar{3}m$ space group. Now to further resolve the structural symmetry in zone 2 temperature range, various possibilities were considered. First it was thought to be sort of structural transition to orthorhombic since some researchers reported the orthorhombic structures of similar double perovskites in recent past [19]. But this consideration was rejected because it is highly unlikely to get such structural transition from low temperature cubic phase with higher symmetry to a relatively lower symmetry orthorhombic phase at higher temperature. Also, in case of cubic-orthorhombic transition, peaks corresponding to (100) plane should split into (100), (010) and

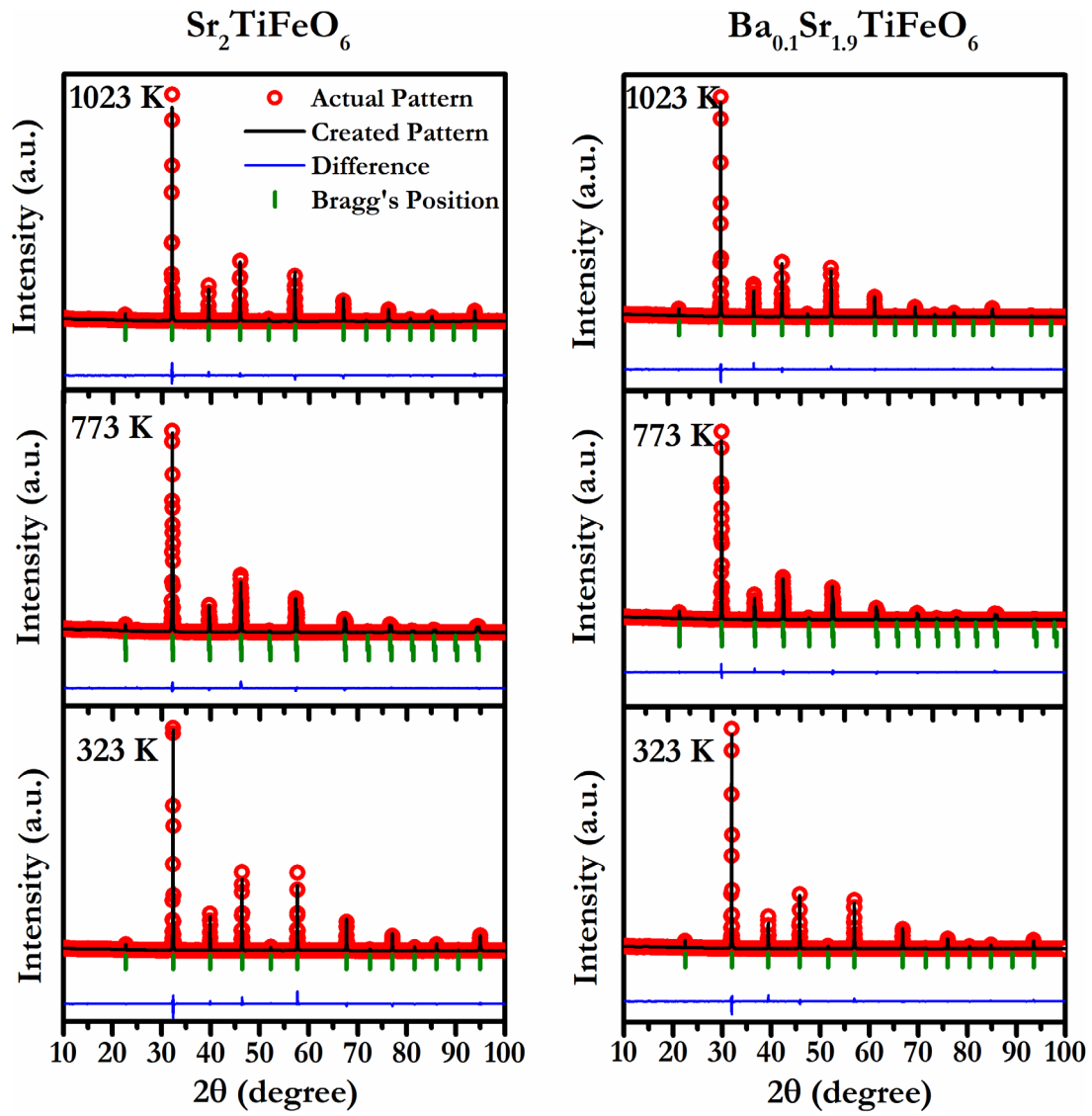


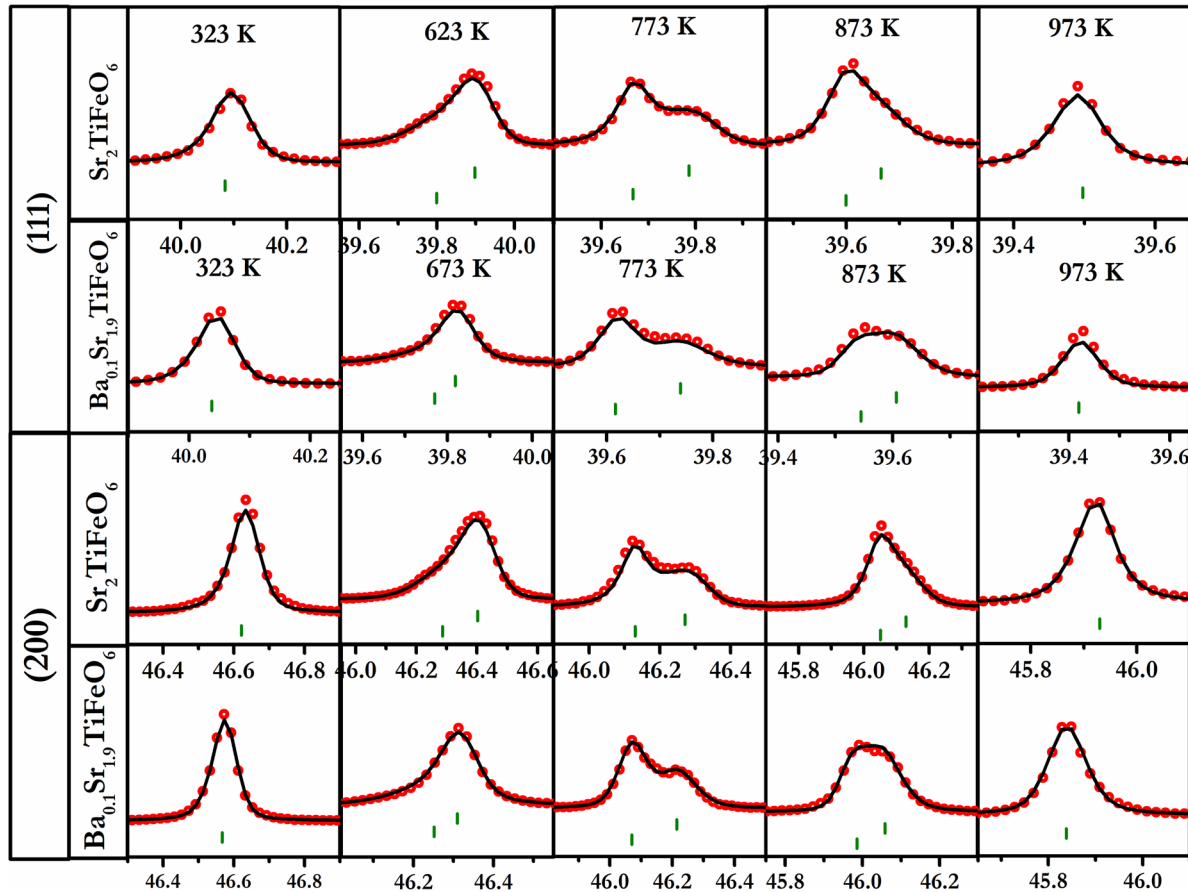
Figure 2. Rietveld refinement plots for STF and BSTF sample at 323 K, 773 K and 1023 K.

Table 1. Wyckoff positions and thermal parameters for rietveld analysis of STF and BSTF compositions at 323 K, 773 K and 1023 K respectively.

Composition	Atoms	Wyckoff positions			B_{iso}			
		X	Y	Z	323 K	773 K		1023 K
					Phase 1	Phase 1	Phase 2	Phase 2
STF	Sr	0.0	0.0	0.0	1.36	1.18	1.68	1.59
	Ti	0.5	0.5	0.5	1.11	0.91	1.53	1.09
	Fe	0.5	0.5	0.5	1.11	0.91	1.53	1.09
	O1	0.5	0.0	0.5	1.52	0.37	1.98	0.96
	O2	0.5	0.5	0.0	1.91	1.99	1.88	1.80
BSTF1	Ba	0.0	0.0	0.0	0.97	1.87	1.57	1.63
	Sr	0.0	0.0	0.0	0.97	1.87	1.57	1.63
	Ti	0.5	0.5	0.5	0.92	1.81	1.55	1.48
	Fe	0.5	0.5	0.5	0.92	1.81	1.55	1.48
	O2	0.5	0.5	0.0	1.73	1.56	0.79	1.06

Table 2. Cell parameters and other reliable parameters for rietveld analysis of STF and BSTF compositions at 323 K, 773 K and 1023 K respectively.

Factors	STF				BSTF1			
	323 K	773 K		1023 K	323 K	773 K		1023 K
		Phase 1	Phase 2			Phase 1	Phase 2	
Cell parameter(Å)	3.9093	3.9209	3.9322	3.9484	3.8973	3.9254	3.9370	3.9559
R _B	5.17	3.15	4.19	3.05	2.60	1.95	2.94	3.79
RF factor	3.38	2.89	3.00	2.31	2.22	1.95	2.37	3.11
χ^2	3.37	1.98		2.29	2.37	1.88		2.12

**Figure 3.** Result of peak fitting using Rietveld refinement method for STF and BSTF for (111) and (200) reflections at various temperatures.

(001), while the reflection corresponding to (110) should split into (110), (101) and (011) since $a \neq b \neq c$; but (111) peak should remain unaltered. However, in our case, all the pseudocubic reflections are found to be split into two, which rules out the possibility of orthorhombic phase. Similarly, the possibility of cubic-tetragonal transition can also be eliminated as diffraction peak corresponding to (111) should remain as singlet for such transition, while (100) and (200) should appear as doublet. Possibilities of rhombohedral and monoclinic structures were also considered; but clear splitting observed in (200) reflection contradicts the possibility of rhombohedral phase, while peak positions were not obtained in case of monoclinic phase. Furthermore, another hypothesis was posited that the double perovskite with stoichiometric formula $\text{Sr}_2\text{TiFeO}_6$ undergoes decomposition into two

single perovskites with stoichiometric formula as SrTiO_3 and SrFeO_3 . Rietveld refinement was carried out on XRD pattern under such consideration. But the phase percentage for the two phases varied with temperature instead of being 50:50. But as the temperature was raised beyond 923 K, Ti:Fe ratio was observed to be 1:1, which makes this hypothesis invalid. Other possibility with oxygen vacancy was also considered where two phases were taken as SrTiO_3 ($Pm\bar{3}m$) and oxygen deficient $\text{SrFeO}_{2.75}$ ($Cmmm$). But for validating the same, XRD patterns should have few other peaks apart from the obtained XRD profiles. Hence, the fitting was not conclusive as we only had peak positions corresponding to cubic perovskite.

But the co-existence of two $Pm\bar{3}m$ cubic phases in zone 2 temperature range is still the viable explanation for such diffraction patterns. Therefore, refinement was carried out

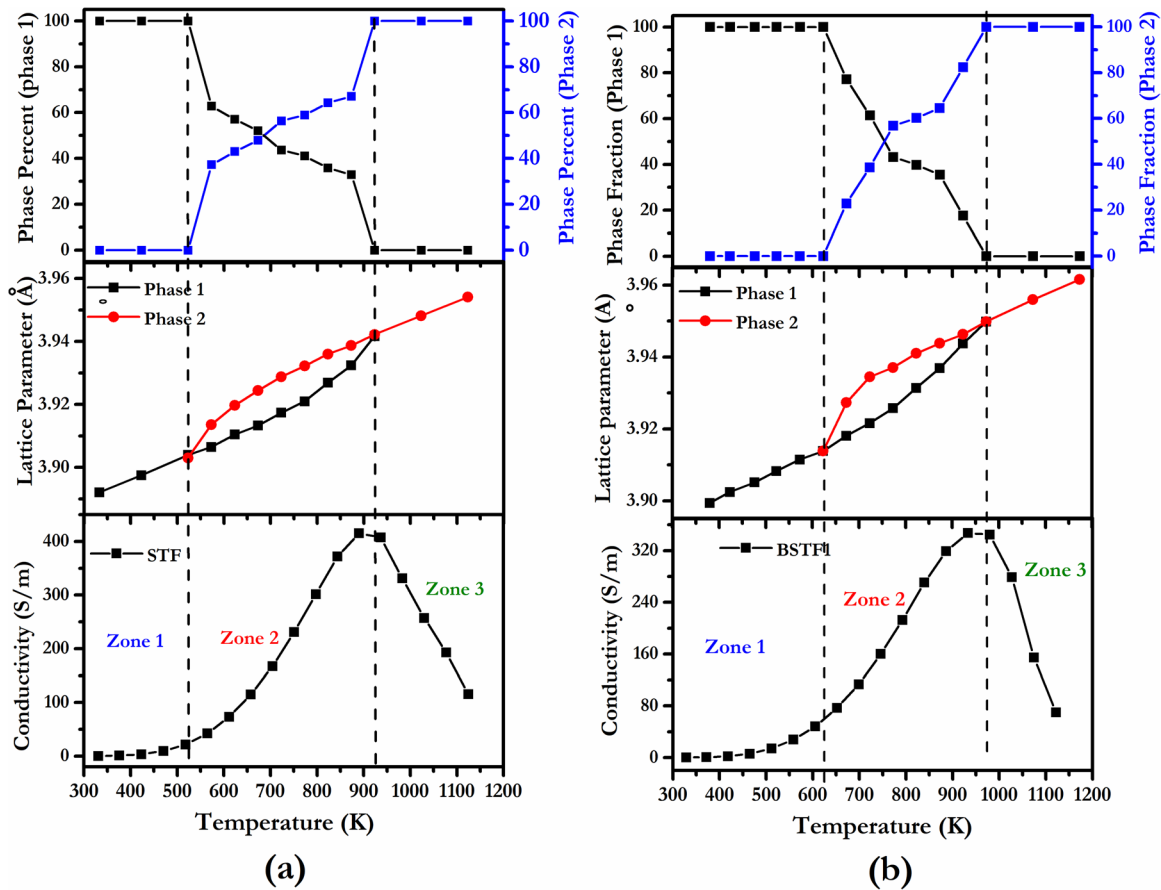


Figure 4. Variation of electrical conductivity, lattice parameters and phase fractions of two co-existing phases with temperature for (a) STF and (b) BSTF.

considering that two types of cubic ($Pm\bar{3}m$) double perovskites with same stoichiometric formula but with different cell dimensions tend to coexist in this temperature region. The refinement results for XRD patterns at 300 K, 773 K and 1023 K are displayed in figure 2 for both the compositions while the Rietveld parameters and atomic position details are presented in tables 1 and 2. It can be observed from the Rietveld plots that for 300 K and 1023 K, each peaks corresponds to single peak position while in case of XRD pattern at 773 K, there is two separate peak positions corresponding to each reflections.

Further, in order to show the goodness of Rietveld refinement fit as well as the compatibility of proposed theory of coexisting two $Pm\bar{3}m$ cubic phases in the intermediate temperature range, refinement results for (111) and (200) pseudocubic reflections for both STF and BSTF at various temperature are shown in figure 3. It is apparent from the XRD profiles shown in figure 3 that both (111) and (200) reflections fit perfectly for single cubic structure ($Pm\bar{3}m$) of STF at 323 K and 1023 K. While a slight shouldering in the left side of both the reflections was observed at 623 K. This smaller reflection on the left side was found to dominate while the contribution of right-side peak was found to be decreased in the pattern of 773 K. With further increase in temperature, the right-side peak appeared as a shoulder in 873 K and finally merged to single cubic phase at 973 K. The similar kind of

behavior was observed in the case of BSTF composition as well. On the basis of this observation, it can be inferred that a new $Pm\bar{3}m$ cubic phase with different cell parameters started to grow in the sample alongside the existing cubic phase beyond a particular temperature, i.e. 573 K for STF and 673 K for BSTF. On further increase in temperature, this newly generated cubic phase started to dominate and at higher temperature it resulted into a single-phase cubic structure e.g. 923 K for STF and 973 K for BSTF compositions.

3.3. Phase coexistence and its effect on electrical property

Figure 4 depicts the variation of electrical conductivity of STF and BSTF double perovskite ceramics along with the variation of lattice parameters and phase fraction with temperature. As discussed in the previous section, the whole data set is divided into three separate zones with different temperature range. For STF, zone 1 lies in the temperature range from 300 K to 523 K in which the conductivity remained almost constant with very low value and the structure remained single cubic phase in this region as shown in figure 4(a). It suggests that the $Pm\bar{3}m$ phase was relatively insulating. For BSTF, zone 1 temperature range varies from 300 K to 623 K. Now, at high temperature region, i.e. zone 3, again a single cubic phase ($Pm\bar{3}m$) reappeared and in this temperature range conductivity was found to be much higher demonstrating metal like behavior ($d\sigma/dT < 0$). It can

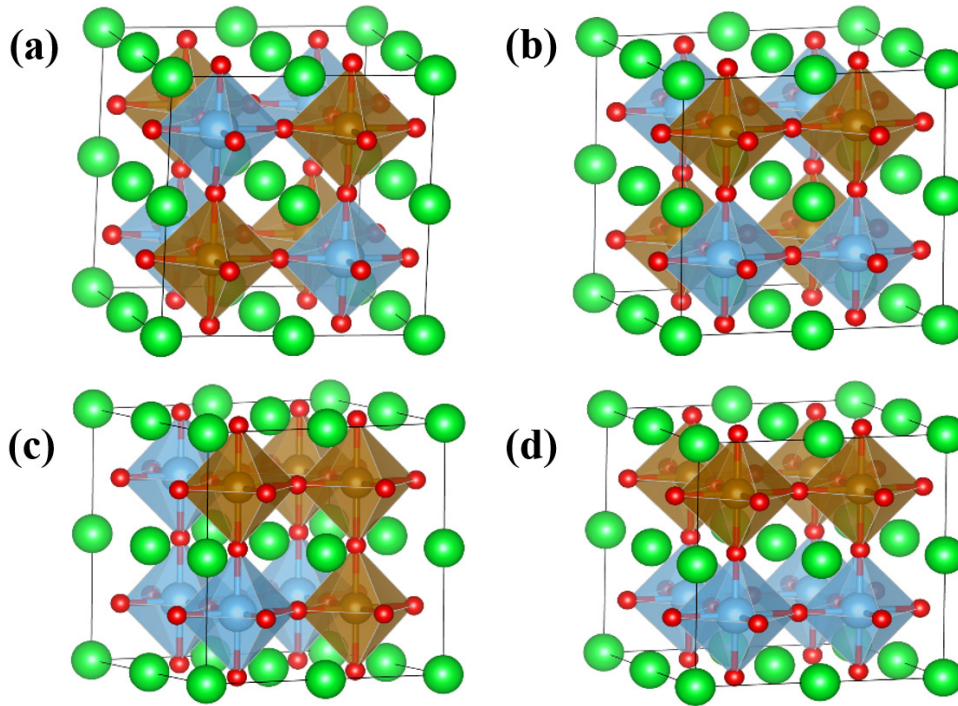


Figure 5. Four types of octahedral arrangements modelled for STF (a) Type 1-rock-salt ordering, (b) Type 2- random $Pm\bar{3}'m$ ordering, (c) Type 3-random $Pm\bar{3}m$ ordering with local clustering and (d) Type 4- layered ordering.

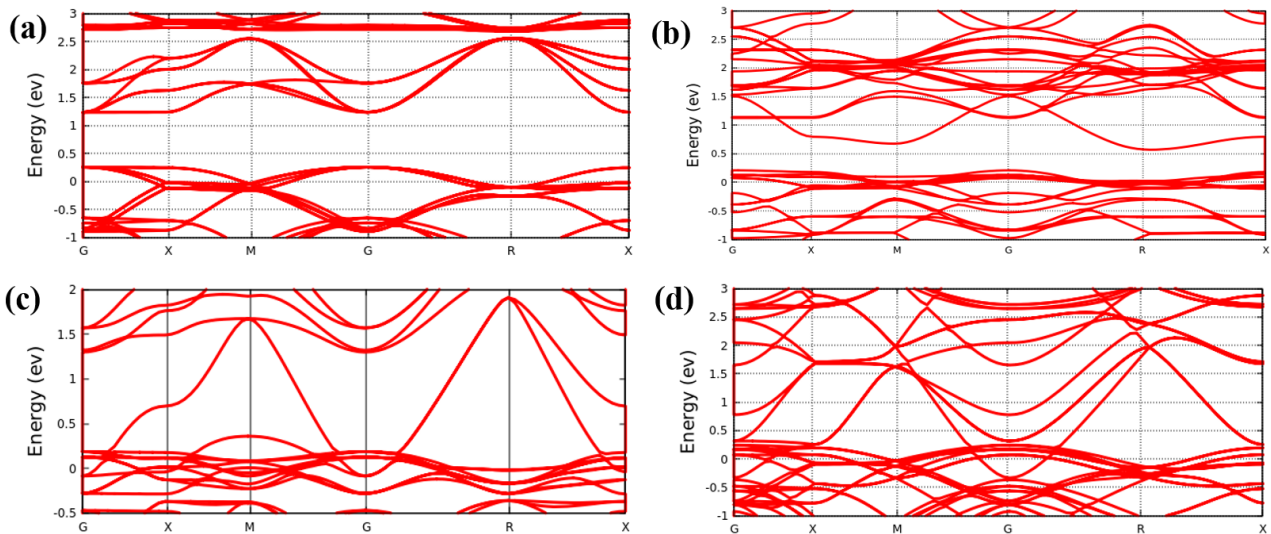


Figure 6. Band structure for (a) Type 1 STF, (b) Type 2 STF, (c) Type 3 STF and (d) Type 4 STF.

be inferred from the present data that the high temperature $Pm\bar{3}m$ cubic phase is relatively highly conducting unlike the insulating $Pm\bar{3}m$ cubic phase observed in zone 1. Zone 3 temperature range varies from 923 K to 1173 K for STF and from 973 K to 1173 K for BSTF. It is well known fact that variation of lattice parameter with temperature for a cubic lattice follows the linear behavior. Although both STF and BSTF showed linear variation in lattice parameters with temperature in zone 1 and zone 3; it can be noted that linear plots in both the regions have different intercepts which rule out the possibility of having similar type of cubic crystal lattice in both the temperature zones. Therefore, it can be assumed that the type of $Pm\bar{3}m$ cubic phase existing in zone 1, designated as

phase 1, was relatively insulating, while the type of $Pm\bar{3}m$ cubic phase existing in zone 3, designated as phase 2, was conducting and responsible for metal-like behavior in the high temperature range.

In zone 2, both the cubic phases were found to be co-existing. It is evident from phase fraction versus temperature plots that phase fraction of phase 1 was 100% in zone one while that of phase 2 was 100% in zone 3. As temperature was increased from zone 1 to zone two, the plot started to show the appearance of a new type of conducting cubic phase i.e. phase 2 with $Pm\bar{3}m$ space group apart from the previously existing low temperature insulator type cubic phase which is phase 1. Now as the temperature was raised, phase fraction

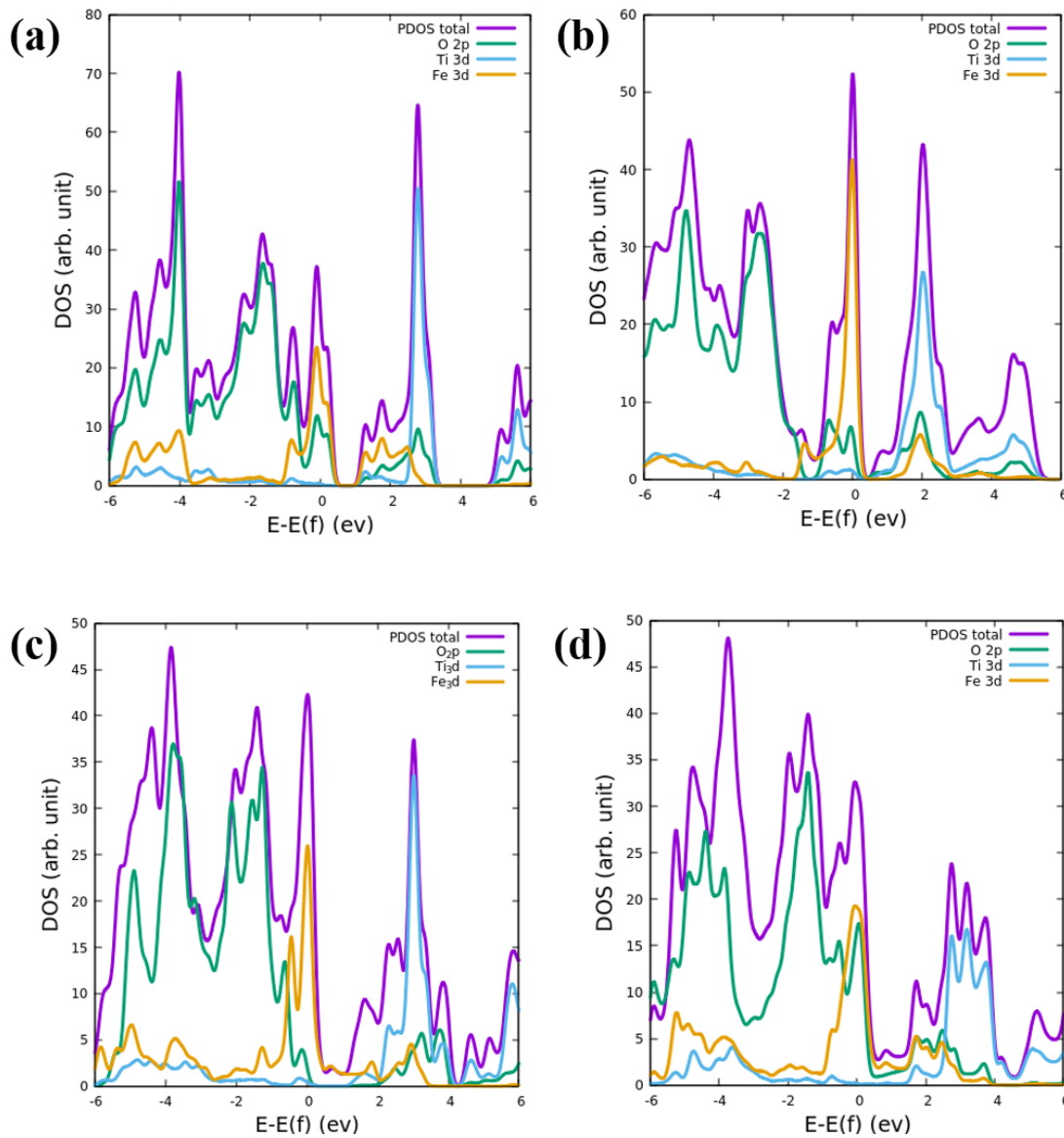


Figure 7. PDOS for (a) Type 1 STF, (b) Type 2 STF, (c) Type 3 STF, (d) Type 4 STF, showing the contributions from 2p orbital of O, 3d orbitals of Ti and Fe.

of the conducting cubic phase 2 was found to be increasing gradually at the expense of previously existing insulator type cubic phase 1, eventually leading to 100% phase fraction of the conducting phase 2 in zone 3. Therefore, the co-existence of a conducting phase 2 alongside non-conducting phase 1 can be attributed for obtaining non-degenerate semiconductor behavior ($d\sigma/dT > 0$) observed in zone 2 compared to insulating behavior exhibited in zone 1 in the conductivity graph. These two cubic phases have same symmetry, $Pm\bar{3}m$ and also contain same sets of atoms. Therefore, it is not possible to predict the difference in these two phases on the basis of XRD analysis. The only possibility causing the electronic restructuring due to these two phases could be the arrangement of oxygen octahedra, contain Fe and Ti atoms, throughout the crystal lattice. Now, the mechanism of separation of one cubic phase in two cubic phase system can be due to simple precipitation and growth of secondary phase with increasing temperature. The simple cubic $Pm\bar{3}m$ orientation

observed at room temperature can be thought to possess a particular octahedral arrangement. But as the temperature was raised, octahedra might have started to reorient themselves locally due to increase in thermal energy, leading to the appearance of another type of cubic phase with same $Pm\bar{3}m$ space group but different cell parameters. It is plausible that as the temperature was increased further, this new high temperature cubic phase started to grow at the expense of other low temperature cubic phase and became primary phase beyond a certain temperature. As the structure is observed to be cubic with $Pm\bar{3}m$ centrosymmetric space group, any possibility of octahedral tilting and ferroelectricity can be ruled out. Furthermore, in order to get better insight on the octahedral arrangement in both the phases and its effect on the electrical behavior of these compositions, theoretical simulation was carried out using DFT to understand band structure of these system which is discussed in details in the following sections.

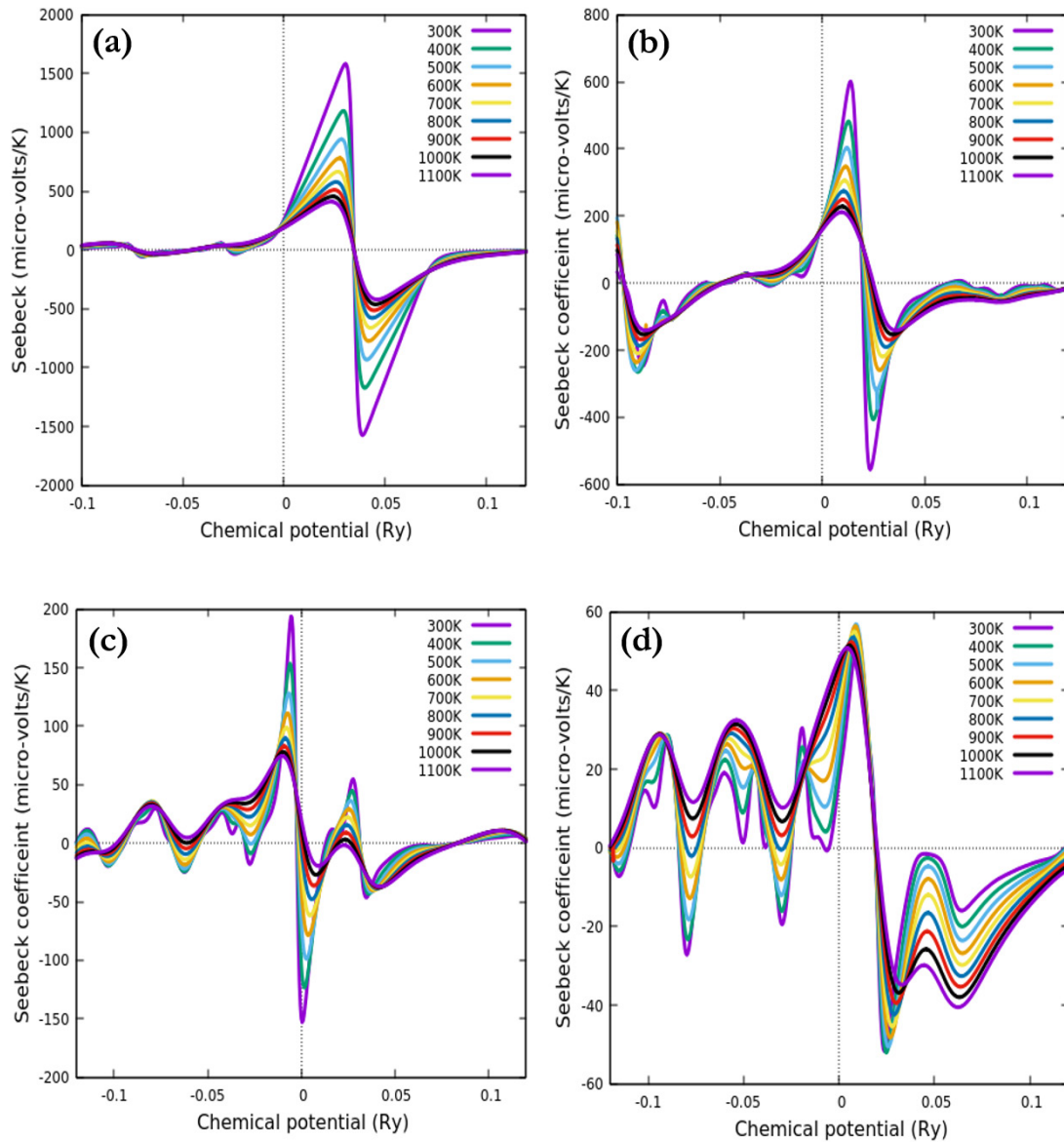


Figure 8. Seebeck coefficient for (a) Type 1 STF, (b) Type 2 STF, (c) Type 3 STF, (d) Type 4 STF, showing variation with respect to chemical potential.

3.4. Octahedral arrangements and Electronic band structure of STF

Since experimental data showed the existence of an insulating and metallic cubic phase at room temperature and high temperature, respectively, several possible arrangements of Ti and Fe octahedra were considered to understand the effect of their arrangements on the electronic band structure as shown in figure 5. We started with a rock-salt ordered structure, where the Ti and Fe octahedra are alternately arranged similar to rock-salt structure (see figure 5(a)). Then we considered two structures, where the Ti and Fe octahedra are arranged randomly and somewhat clustered, shown in figures 5(b) and (c), respectively. Finally, we also considered a layered arrangement of Ti and Fe octahedra (see figure 5(d)), completely separating them from each other. It is well known that Fe tends to exist in the +3 oxidation state. Hence, oxygen vacancies are bound to exist and we took this into account while calculating

the electronic band structure, by creating two oxygen vacancies per super cell. Calculated electronic band structures are shown in figure 6.

As shown in the figure, in case of STF, the Fermi level either lies in the valence band (figures 6(a) and (b)) or there exists no bandgap (figures 6(c) and (d)). In case of figures 6(a) and (b), there exist a gap of magnitude 0.95 and 0.33 eV, respectively, in the energy spectrum of STF, although the magnitude of the gap is significantly less compared to the SrTiO₃ (LDA bandgap to be equal to 1.86 eV). Note that, Fermi level lying in the valence band indicates positive charge carriers or holes, which is consistent with the experimental data of STF.

Further analysis was carried out in terms of atomic orbital projected density of states (PDOS), which clearly illustrates the dominance of Fe-3d states near the Fermi level, irrespective of the crystal structure of STF, as shown in figure 7. As shown in the diagram, the other orbital having significant contribution is O-2p, while Ti-3d states have negligible contribution

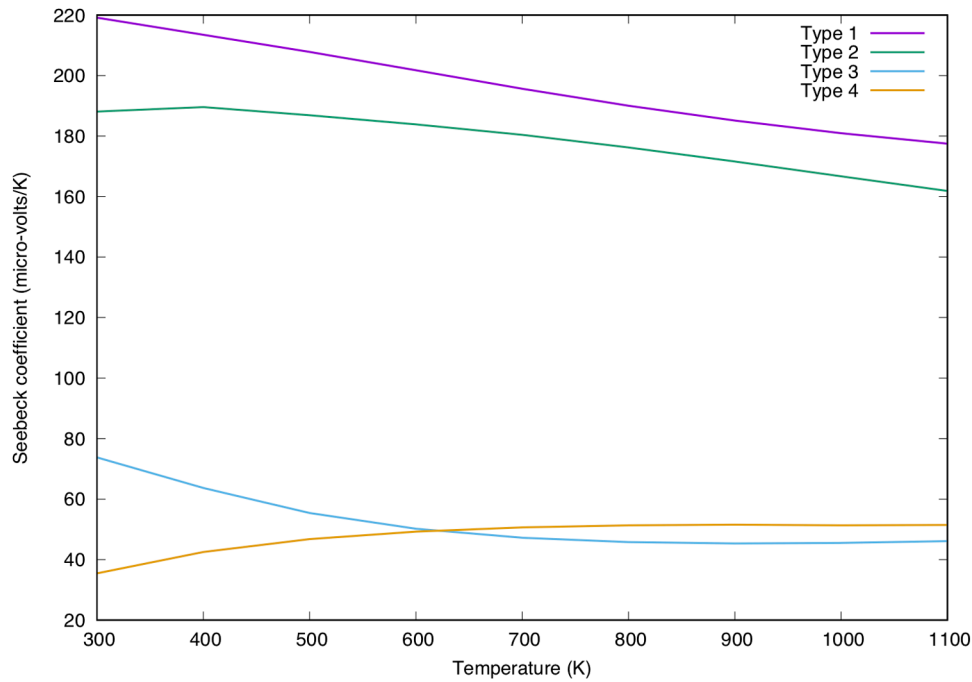


Figure 9. Calculated Seebeck coefficient in the temperature range from 300 K to 1100 K for STF with four different types of octahedral arrangements.

near the Fermi level. Note that, in case of type-2 and type-3 STF, contributions of Fe-3d orbitals are far more significant than O-2p states, while the latter has noticeable weightage in case of type-1 and type-4 STF. In summary, Fe-3d states play an important role in electronic transport of STF, where conduction is mainly via positive charge carriers or holes.

Out of the four possible configurations studied so far, the rock-salt structure is unlikely to occur because it belongs to the $Fm\bar{3}m$ space group [20] while, $Pm\bar{3}m$ was the experimentally observed space group. Moreover, no such super lattice peaks were observed in the XRD data, hence the possibility of having $Fm\bar{3}m$ structure can be ignored. The layered configuration is also less likely based on the same argument that such a structure cannot have $Pm\bar{3}m$ space group. Moreover, STF also does not satisfy the Anderson's criteria of layering in double perovskites [4]. Also, simulated XRD patterns for type 2 and type 3 STF showed $Pm\bar{3}m$ space group symmetry shown in figure (S2) (stacks.iop.org/JPhysCM/32/235401/mmedia), which corroborates well with the experimental results.

However, the possibility of local layering of Ti and Fe octahedra, especially at higher temperatures, cannot be ruled out completely because the layered configuration relaxed into a tetragonal structure with a c/a ratio of 1.005, which is too low to be detected in the XRD. Thus, perfectly ordered crystals, either in the form of a rock-salt structure, or a configuration with separate Fe and Ti layers, are less likely and what we observed in experiments are possibly less ordered structures of $Pm\bar{3}m$ space group, like type 2 and type 3 configuration, as illustrated in figures 5(b) and (c). As shown in figures 6(b) and (c), even for less ordered type 2 and type 3 crystals, electronic band structure depends significantly on the distribution of Fe and Ti polyhedra. In order to understand whether oxygen vacancies play any role, we also compare the electronic band

structure, with and without O-vacancies, for type 2 and type 3 STF. We have found that, the electronic band structure of type 2 STF weakly depends on the number of oxygen vacancies. On the other hand, there is hardly any effect of number of oxygen vacancies on electronic band structure of type 3 STF (more detailed information is given in the supporting information). This further proves that Fe is playing a major role in the conduction process of STF, while O-vacancies may not be having any significant role. While O-vacancies can contribute some electrons, their numbers are not too high, because hole conduction is experimentally observed in STF as evident from positive Seebeck coefficient observed in the whole temperature range of measurement, shown in figure S5. Thus, as Fe-3d states dominate near the Fermi level, a connected framework of Fe polyhedra form a conduction path in case of type 3 structure. Further, we calculated electrical conductivity (using relaxation time approximation) of Type 2 and Type 3 STF. The results are shown in the figure S6 in supporting information. It is evident that Type-3 STF has higher conductivity than that of Type-2, which corroborates well the experimental observation. Moreover, we calculated the transport properties for all the structures for qualitative understanding, as described in the next section.

3.5. Transport properties of STF

Using the constant relaxation time approximation, as implemented in the BoltzTraP code, we calculated thermoelectric properties of STF. The calculated Seebeck coefficient versus chemical potential is plotted for the temperature range from 300 K to 1100 K for all the 4 possible configurations as shown in figure 8. The value at $\mu = 0$ gives the value for the Seebeck coefficient at a given temperature. Figure 9 shows the plot for

calculated Seebeck coefficient varied with temperature for all the 4 types of configurations. Since Type 2 and Type 3 arrangements are the possible crystal structures of STF, we compared the calculated Seebeck coefficients for these particular configurations with the experimental values. In case of Type 2, calculated value of Seebeck coefficient was found to be around $188 \mu\text{V K}^{-1}$, which is very close to the experimental value obtained. In case of Type 3, which showed metal-like behavior from the band structure calculations, a very low Seebeck coefficient was predicted by our calculations. However, in reality there are various scattering mechanisms that are not taken into account by BoltzTraP and hence the sharp rise in the Seebeck coefficient that was obtained experimentally beyond 923 K could not be predicted theoretically.

Because Ba and Sr belong to the same group and in consecutive periods, hence not much change expected in the properties due to Ba doping. However, we calculated the band structure by DFT and estimated the Seebeck coefficient by BoltzTraP for BSTF double perovskite as well. As expected, we got the similar conclusion as shown in the supporting information.

4. Conclusion

In conclusion, we investigated the reason behind semiconductor to metal-like transition observed in the temperature dependent electrical conductivity behavior of $\text{Ba}_{1-x}\text{Sr}_x\text{TiFeO}_6$ (BSTF) double perovskites using high temperature XRD analysis in conjugation with DFT study. Rietveld refinement of high temperature XRD data shows that BSTF preserves its room temperature single cubic phase with $Pm\bar{3}m$ space group upto 523–632 K. Also, beyond 923 K, a single cubic phase ($Pm\bar{3}m$) prevails, which is highly conductive in nature in contrast to the insulator like cubic phase detected at room temperature. Moreover, Rietveld refinement of XRD data in correlation with electrical conductivity behavior of BSTF suggests the co-existence of conducting and insulating phases having similar cubic structure ($Pm\bar{3}m$) in the intermediate temperature range resulting the semiconductor ($d\sigma/dT > 0$) to metal like ($d\sigma/dT < 0$) transition observed in these double perovskites. Further to study the electronic restructuring happened possibly due to the octahedral re-arrangements, DFT simulations were performed. Considering 4 possible octahedral arrangements available in a $2 \times 2 \times 2$ periodic box containing 40 atoms, the band gap was found to be reduced as the clustering of Fe ions increased to the point that the ordering of Ti and Fe ions showed metallic character. Existence of predominantly randomly-oriented octahedra (Type 2) configuration is verified computationally in the low temperature region where there is minimal rise in conductivity with temperature indicating insulator-like behavior. At high temperature the decrease in conductivity with temperature was found to be due to the existence of locally clustered octahedra configuration (Type 3), which showed metallic like band structure.

BoltzTraP provided values for the Seebeck coefficient, which are in good agreement with the experimental values for most of the temperature range.

Acknowledgment

This work is supported by the grant from Science and Engineering Research Board, DST (SERB-DST), India (Grant No: IMP/2018/000955 and SB/S3/ME/008/2015).

ORCID iDs

Akansha Dwivedi  <https://orcid.org/0000-0002-6494-1681>
Tanmoy Maiti  <https://orcid.org/0000-0003-1581-7614>

References

- [1] Vasala S and Karppinen M 2015 $A_2B'B''O_6$ perovskites: a review *Prog. Solid State Chem.* **43** 1–36
- [2] Pickett W E and Singh D J 1997 Chemical disorder and charge transport in ferromagnetic manganites *Phys. Rev. B* **55** R8642
- [3] Meetei O N, Erten O, Mukherjee A, Randeria M, Trivedi N and Woodward P 2013 Theory of half-metallic double perovskites. I. Double exchange mechanism *Phys. Rev. B* **87** 165104
- [4] Andreson M T, Greenwood K B, Taylor G A and Poppelmeier K R 1993 B-cation arrangements in double perovskite *Prog. Solid State Chem.* **22** 197–233
- [5] Maiti T, Saxena M and Roy P 2019 Double perovskite ($\text{Sr}_2\text{B}'\text{B}''\text{O}_6$) oxides for high-temperature thermoelectric power generation—a review *J. Mater. Res.* **34** 107–25
- [6] Roy P, Waghmare V and Maiti T 2016 Environmentally friendly $\text{Ba}_x\text{Sr}_{2-x}\text{TiFeO}_6$ double perovskite with enhanced thermopower for high temperature thermoelectric power generation *RSC Adv.* **6** 54636–43
- [7] Roy P, Bose I and Maiti T 2016 Synthesis and characterization of Sr_2TiMO_6 ($M = \text{Fe}, \text{Co}$) double perovskites for high temperature thermoelectric applications *Integr. Ferroelectr.* **174** 34–42
- [8] Saxena M, Roy P, Acharya M, Bose I, Tanwar K and Maiti T 2016 Enhanced thermoelectric figure-of-merit in environmentally benign $\text{Ba}_x\text{Sr}_{2-x}\text{TiCoO}_6$ double perovskites *Appl. Phys. Lett.* **109** 263903
- [9] Saxena M and Maiti T 2017 Effect of Ba-doping on high temperature thermoelectric properties of $\text{Sr}_2\text{TiMoO}_6$ double perovskites *J. Alloys Compd.* **710** 472–8
- [10] Roy P, Waghmare V, Tanwar K and Maiti T 2017 Large change in thermopower with temperature driven p-n type conduction switching in environment friendly $\text{Ba}_x\text{Sr}_{2-x}\text{Ti}_{0.8}\text{Fe}_{0.8}\text{Nb}_{0.4}\text{O}_6$ double perovskites *Phys. Chem. Chem. Phys.* **19** 5818–29
- [11] Rowe D M 2018 *Thermoelectrics Handbook: Macro to Nano* (Boca Raton, FL: CRC Press)
- [12] Liu X J, Moritomo Y, Nakamura A and Kojima N 1999 Pressure-induced phase transition in mixed-valence gold complexes $\text{Cs}_2\text{Au}_2\text{X}_6$ ($X = \text{Cl}$ and Br) *J. Chem. Phys.* **110** 9174–8
- [13] Lin J, Chen H, Gao Y, Cai Y, Jin J, Etman A S, Kang J, Lei T, Lin Z and Folgeruas M C 2019 Pressure-induced

- semiconductor-to-metal phase transition of a charge-ordered indium halide perovskite *Proc. Natl Acad. Sci.* **116** 23404–9
- [14] Kang C-J and Kotliar G 2019 Material design of indium-based compounds: Possible candidates for charge, valence, and bond disproportionation and superconductivity *Phys. Rev. Mater.* **3** 15001
- [15] Giannozzi P, Baroni S, Bonini N, Calandra M, Car R, Cavazzoni C, Ceresoli D, Chiarotti G L, Cococcioni M and Dabo I 2009 Quantum espresso: a modular and open-source software project for quantum simulations of materials *J. Phys.: Condens. matter* **21** 395502
- [16] Perdew J P, Burke K and Ernzerhof M 1996 Generalized gradient approximation made simple *Phys. Rev. Lett.* **77** 3865
- [17] Reihl B, Bednorz J G, Müller K A, Jugnet Y, Landgren G and Morar J F 1984 Electronic structure of strontium titanate *Phys. Rev. B* **30** 803–6
- [18] Madsen G K H and Singh D J 2006 BoltzTraP. A code for calculating band-structure dependent quantities *Comput. Phys. Commun.* **175** 67–71
- [19] Shankar U, Agarwal P K, Pandey R and Singh A K 2016 Investigation of crystal structure of SrLa(FeTi)O₆ and BaLa(FeTi)O₆ perovskites by rietveld refinement *Solid State Sci.* **52** 78–82
- [20] Samanta K and Saha-Dasgupta T 2017 Rocksalt versus layered ordering in double perovskites: a case study with La₂CuSnO₆ and La₂CuIrO₆ *Phys. Rev. B* **95** 235102